Mon. Not. R. Astron. Soc. **000**, **??**–**??** (2009w) Printed 20 February 2024 (MN LATEX style file v2.2)

Evolution of the Dark Matter Phase-Space Density Distributions of CDM Halos

Ileana M. Vass[1,2], Monica Valluri[2,3?], Andrey V. Kravtsov[2,4,5], Stelios Kazantzidis[6]
[1] *Department of Astronomy University of Florida, Gainesville, FL 32611, USA*
[2] *Kavli Institute for Cosmological Physics, The University of Chicago, Chicago, IL 60637, USA,*
[3] *Department of Astronomy, University of Michigan, Ann Arbor, MI 48109, USA,* mvalluri@umich.edu
[4] *Enrico Fermi Institute, The University of Chicago, Chicago, IL 60637, USA*
[5] *Dept. of Astronomy & Astrophysics, The University of Chicago, 5640 S. Ellis Ave., Chicago, IL 60605*
[6] *Center for Cosmology and Astro-Particle Physics, The Ohio State University, Columbus, OH 43210, USA*

Accepted 2009 Feburary 4; Received 2009 February 2; in original form 2008 October 1

ABSTRACT

We study the evolution of phase-space density during the hierarchical structure formation of CDM halos. We compute both a spherically-averaged surrogate for phase-space density ($Q = = ^3$) and the coarse-grained distribution function $f(x;v)$ for dark matter particles that lie within 2 virial radii of four Milky-Way-sized dark matter halos. The estimated $f(x;v)$ spans over four decades at any radius. Dark matter particles that end up within two virial radii of a Milky-Way-sized DM halo at $z = 0$ have an approximately Gaussian distribution in $\log(f)$ at early redshifts, but the distribution becomes increasingly skewed at lower redshifts. The value f_{peak} corresponding to the peak of the Gaussian decreases as the evolution progresses and is well described by $f_{peak}(z) / (1+z)^{4:5}$ for $z > 1$. The highest values of f, (responsible for the skewness of the profile) are found at the centers of dark matter halos and subhalos, where f can be an order of magnitude higher than in the center of the main halo. We confirm that $Q(r)$ can be described by a power-law with a slope of $1:8 \quad 0:1$ over 2.5 orders of magnitude in radius and over a wide range of redshifts. This $Q(r)$ profile likely reflects the distribution of entropy ($K \quad ^2 = ^{2=3}_{dm} / r^{1:2}$), which dark matter acquires as it is accreted onto a growing halo. The estimated $f(x;v)$, on the other hand, exhibits a more complicated behavior. Although the median coarse-grained phase-space density profile $F(r)$ can be approximated by a power-law, $/ r^{1:6 \quad 0:15}$, in the inner regions of halos ($< 0:6\, r_{vir}$), at larger radii the profile flattens significantly. This is because phase-space density averaged on small scales is sensitive to the high-f material associated with surviving subhalos, as well as relatively unmixed material (probably in streams) resulting from disrupted subhalos, which contribute a sizable fraction of matter at large radii.

1 INTRODUCTION

Cosmological N-body simulations of the formation of structure in the Universe allow us to reconstruct how gravitationally bound objects like galaxies and clusters form and evolve. These simulations have shown that despite the seemingly complex hierarchical formation history of dark matter (DM) halos, the matter density distributions of cosmological DM halos are described by simple 3-parameter profiles (Navarro et al. 1996; Merritt et al. 2006).

The study of the evolution of the phase-space distribution function (DF) of a collisionless dynamical system (composed of stars or DM or both) is fundamental to understanding its dynamical evolution, since a collisionless system is completely described by its phase-space density distribution (otherwise called the fine-grained DF $f(x;v)$). For an isolated collisionless system, $f(x;v;t)$ is fully described by the Collisionless Boltzmann Equation (CBE) (sometimes called the Vlasov equation), which is a continuity equation in phase-space. A consequence of the CBE is that the fine-

grained DF is always conserved. In addition, $V(f)df$, the volume of phase-space occupied by phase-space elements whose density lies between $(f; f + df)$, is also conserved. However, the conservation of the fine-grained $f(x;v)$ and $V(f)df$ is not a very useful property for understanding the evolution of real systems, since in practice it is only possible to compute an average of f over a finite volume of phase-space. This average is referred to as the coarse-grained DF $f(x;v)$, and the associated volume density is $V(f)$. The evolution of the coarse-grained DF is governed by *Mixing Theorems* (Binney & Tremaine 1987; Tremaine et al. 1986; Mathur 1988). These theorems state that if the coarse-grained DF is bounded, then processes that operate during the relaxation of collisionless systems (e.g. phase mixing, chaotic mixing, and the mixing of energy and angular momentum that accompanies violent relaxation) result in a decrease in the coarse-grained phase-space density. This is because at any point in phase-space, both low and high phase-space density regions get highly mixed (Binney & Tremaine 1987; Tremaine et al. 1986). In addition, there are simple relationships that exist between the initial $V(f)$ and the coarse-grained $V(f)$ at a later time: $V(f)$ is always greater than $V(f)$ (Mathur 1988).

Recently, Dehnen (2005) proved a new Mixing Theorem that states that the excess-mass function $D(f)$, which is the mass of material with coarse-grained phase-space density greater than a value f, always decreases due to mixing, for all values of f. He showed, using this theorem, that steeper cusps are less mixed than shallower ones, independent of the details of the DF or density profile, and this implies that a merger remnant cannot have a cusp that is either steeper or shallower than the steepest of its progenitors.

Taylor & Navarro (2001) have introduced a surrogate quantity, $Q(r) = (r)=(r)^3$, where (r) is the configuration-space density averaged in spherical shells, and (r) is the velocity dispersion of DM particles averaged in a spherical shell centered at the radius r. Note that, although $Q(r)$ has dimensions of phase-space density, it is *not* true coarse-grained phase-space density, because it is constructed out of separately computed configuration-space density and velocity dispersion in arbitrarily chosen spherical shells. Consequently, it is not expected to obey any *Mixing Theorems* (Dehnen & McLaughlin 2005) and is generally difficult to interpret in terms of phase-space density. Nevertheless, it is an intriguing quantity, because Taylor & Navarro (2001) show that $Q(r)$ is well approximated by a single power-law, Q / r with $1:874$ over more than 2.5 orders of magnitude in radius for CDM halos universally, regardless of mass and background cosmology (see also Rasia et al. 2004; Ascasibar et al. 2004). Recent work, however, indicates that $Q(r)$ profiles are somewhat sensitive to the amount of substructure and the slope of the power spectrum (Wang & White 2008; Knollmann et al. 2008).

While power-law $Q(r)$ profiles are by no means universal for self-gravitating systems in dynamical equilibrium (Barnes et al. 2006), power-law profiles with exactly the same slope were first shown to arise in simple self-similar spherical gravitational infall models (Bertschinger 1985) pointing to a possible universality in the mechanisms that produces them. Austin et al. (2005) extended the early work of Bertschinger (1985) using semi-analytical extended secondary infall models to follow the evolution of collisionless spherical shells of matter that are initially set to be out of dynamical equilibrium and are allowed to move only radially. They concluded that the power-law behavior of the final phase-space density profile is a robust feature of virialized halos, which have reached equilibrium via violent relaxation. They used a constrained Jeans equation analysis to show that this equation has different types of solutions and that it admits a unique periodic solution which gives a power-law density profile with slope $= 1:9444$ (comparable to the numerical value of $= 1:87$ obtained by Taylor & Navarro (2001)).

A recent study by Hoffman et al. (2007) followed the evolution of $Q(r)$ profiles in cosmological DM halos in constrained simulations designed to control the merging history of a given halo. These authors showed that, during relatively quiescent phases of halo evolution, the density profile closely follows that of a NFW halo, and $Q(r)$ is always well represented by a power-law r with $= 1:9 \quad 0:1$. They showed that $Q(r)$ deviates from power-law most strongly during major mergers but recovers the power-law form thereafter (this is consistent with our findings using a series of controlled merger simulations, Vass et al. 2009). More recently, Wojtak et al. (2008) demonstrated (using a variant of the FiEstAS code) that the DF of CDM halos of mass $10^{14} \quad 10^{15}$ M can be separated into energy and angular momentum components. They proposed a phenomenological model for spherical potentials and showed that their model DF was a good match to the N-body DFs and was also able to reproduce the power-law behavior of $Q(r)$. Another study of relevance is the work of Peirani & de Freitas Pacheco (2007), which defined a global value for the phase-space density, Q, which they found decreases rapidly with time. Despite the insights obtained in these studies, the origin for the universality of $Q(r)$ is not yet understood, and the question of how this quantity relates to the true coarse-grained phase-space density has not yet been thoroughly investigated. This motivates our study which is focused on the evolution of *both* $Q(r)$ and phase-space density evolution using a set of self-consistent cosmological simulations of halo formation.

In the last four years, three independent numerical codes to compute the true coarse-grained phase-space density from N-body simulations have been developed (Arad et al. 2004; Ascasibar & Binney 2005; Sharma & Steinmetz 2006). In the Appendix we compare results obtained with the codes "FiEstAS" (Ascasibar & Binney 2005) and "EnBiD" (Sharma & Steinmetz 2006) at a range of redshifts. However we only present results obtained with the "EnBiD" code using a specific kernel. Following the submission of this paper we became aware of the work of Maciejewski et al. (2008). These authors carried out a similar comparison of various coarse-grained phase space density estimators for N-body simulations cosmological halos at $z = 0$.

In an accompanying paper (Vass et al. 2009), we present analysis of phase-space and $Q(r)$ evolution during major mergers between CDM-like spherical halos. We show that major mergers (those which are the most violent and therefore likely to result in the greatest amount of mixing in phase-space) preserve spherically-averaged phase-space density profiles (both $Q(r)$ and $F(r)$) out to the virial radius r_{vir} of the final remnant. We confirm the prediction (Dehnen 2005) that the phase-space density profiles of DM halos are extremely robust, and in particular, the prediction that the steepest central cusp always survives.

To understand the robustness of profiles outside the central cusp (Vass et al. 2009), we drew on recent work by Valluri et al. (2007) that shows that matter in equally-spaced radial shells is redistributed during the merger is such a way that only about 20% of the matter in the central cusp is ejected during the merger to radii extending out to about two scale radii. For all other radii, roughly 15% by mass in each radial shell is redistributed uniformly with radius. Further, nearly 40% of the mass of the progenitor halos lies beyond the formal virial radius of the remnant (Kazantzidis et al. 2006; Valluri et al. 2007), and this matter originates roughly uniformly from each radial interval starting from about three scale radii from the center. While major mergers (such as those studied by Dehnen 2005; Vass et al. 2009) are instructive, they represent the most extreme form of mixing, and are not the major mode of mass accretion in the Universe. In addition, since experiments with major mergers demonstrate that pre-existing power-law profiles are preserved, they shed little light on the formation of the profiles. Our primary goal is to gain a better understanding of the origin of the power-law phase-space density profiles seen in cosmological DM simulations.

In this paper we investigate the evolution of the coarse-grained phase-space density in the formation and evolution of four Milky-Way-sized halos in a CDM cosmology with cosmological parameters: $(\ _m\ ;\ \ ;h;\ _8) = (0{:}3;0{:}7;0{:}7;0{:}9)$. In x 2 we summarize the cosmological N-body simulations analyzed in this study as well as the numerical methods used to obtain coarse-grained phase-space densities. (The Appendix contains a detailed comparison of the two codes FiEstAS and EnBiD . We also present reasons for our choice of EnBiD , with a $n = 10$ smoothing kernel). In x 3 we describe the properties of the spherically-averaged quantity $Q(r)$ as well as the the coarse-grained DF for one Milky-Way-sized DM halo at $z = 0$, as well as the evolution of the phase-space DF of this halo from $z = 9$ to the present. In x 4 we also present results for three additional Milky-Way-sized halos. In x 5 we present an interpretation of the power-law profiles seen in $Q(r)$ and discuss the implications of observed coarse grained distribution function in a cosmological context. x 6 summarizes the results of this paper and concludes.

2 NUMERICAL METHODS

The simulations analyzed in this paper are described in greater detail in the works of Kravtsov et al. (2004) and Gnedin & Kravtsov (2006). The simulations were carried out using the Adaptive Refinement Tree N -body code (ART Kravtsov et al. 1997). The simulation starts with a uniform 256^3 grid covering the entire computational box. This grid defines the lowest (zeroth) level of resolution. Higher force resolution is achieved in the regions corresponding to collapsing structures by recursive refining of all such regions by using an adaptive refinement algorithm. Each cell can be refined or de-refined individually. The cells are refined if the particle mass contained within them exceeds a certain specified value. The grid is thus refined to follow the collapsing objects in a quasi-Lagrangian fashion.

Three of the galactic DM halos were simulated in a comoving box of 25 h^{-1} Mpc (hereafter L25); they were selected to reside in a well-defined filament at $z = 0$. Two halos are neighbors, located 425 h^{-1} kpc from each other. The third halo is isolated and is located two Mpc away from the pair. Hereafter, we refer to the isolated halo as G_1 and the halos in the pair as G_2 and G_3. Although we analyzed all three halos at the same level of detail we present detailed results for G_1. The virial masses and virial radii for the halos studied are given in Table 1 in Kravtsov et al. (2004). The virial radius (and the corresponding virial mass) was chosen as the radius encompassing a mean density of 200 times the mean density of the Universe. The masses of the DM halos are well within the range of possibilities allowed by models for the halo of the Milky Way galaxy (Klypin et al. 2002). The simulations followed a Lagrangian region corresponding to the sphere of radius equal to two virial radii around each halo at $z = 0$. This region was re-sampled with the highest resolution particles of mass $m_p = 1{:}2 \quad 10^6 h^{-1} M$, corresponding to 1024^3 particles in the box, at the initial redshift of the simulation ($z_i = 50$). The maximum of ten refinement levels was reached in the simulations corresponding to the peak formal spatial resolution of $152 h^{-1}$ parsec. Each host halo is resolved with 10^6 particles within its virial radius at $z = 0$.

The fourth halo was simulated in a comoving box of 20 h^{-1} Mpc box (hereafter L20), and it was used to follow the Lagrangian region of approximately five virial radii around the Milky Way-sized halo with high resolution. In the high-resolution region the mass of the DM particles is $m_p = 6{:}1 \quad 10^5 h^{-1} M$, corresponding to effective 1024^3 particles in the box, at the initial redshift of the simulation ($z_i = 70$). As in the other simulation, this run starts with a uniform 256^3 grid covering the entire computational box. Higher force resolution is achieved in the regions corresponding to collapsing structures by recursive refining of all such regions using an adaptive refinement algorithm. Only regions containing highest resolution particles were adaptively refined. The maximum of nine refinement levels was reached in the simulation corresponding to the peak formal spatial resolution of $150 h^{-1}$ comoving parsec. The Milky Way-sized host halo has the virial mass

of $1{:}4 \quad 10^{12} h^{-1} M$ (or $2{:}3$ million particles within the virial radius) and virial radius of $230 h^{-1}$kpc at $z = 0$.

The peak spatial resolution of the simulations determines the minimum radius to which we can trust the density and velocity profiles. In the following analysis, we only consider profiles at radii at least eight times larger than the peak resolution of the simulations (i.e., $0{:}5 \quad 0{:}6 h^{-1}$ comoving kpc or $r \quad 0{:}004\, r_{vir(z=0)}$).

2.1 Phase-space density estimators

In this paper, we will focus on the time evolution of the spherically averaged phase-space density $Q(r)$ as well as the coarse-grained phase-space DF $f(x;v)$ during the formation of the Milky-Way sized DM halos in CDM cosmological simulations described above.

In the last four years three independent numerical codes to compute the coarse-grained phase-space density from N-body simulations have been developed (Arad et al. 2004; Ascasibar & Binney 2005; Sharma & Steinmetz 2006)[1]. These techniques differ in the scheme used to tesselate 6-dimensional phase space as well as in the density estimators they use. The first study of coarse grained DF (Arad et al. 2004) showed that it has its highest values at the centers of DM halos and subhalos. They also showed that the volume density of phase-space $V(f)$ within individual cosmological DM halos at $z = 0$ has a power-law profile over nearly four orders of magnitude in f. The main criticism of this code is that it is not metric-free. The FiEstAS algorithm of Ascasibar & Binney (2005) and the EnBid algorithm of Sharma & Steinmetz (2006) are preferred due to their speed and the metric free nature. The FiEstAS algorithm is based on a repeated division of each dimension of phase-space into two regions that contain roughly equal numbers of particles. EnBiD (Sharma & Steinmetz 2006) closely follows the method used in FiEstAS, but it optimizes the number of divisions to be made in a particular dimension by using a minimum-entropy criterion based on the *Shannon entropy* that measures the phase-space density with much greater accuracy when f is high. Sharma & Steinmetz (2006) showed that EnBiD with a kernel which includes 10 nearest neighbors ($n = 10$) about each point was able to recover analytic phase-space density profiles to nearly 3-4 decades higher values of f than FiEstAS.

[1] An even more sophisticated numerical method has recently been presented by Vogelsberger et al. (2008) for calculating the fine-grained phase-space structure of DM distributions derived from cosmological simulations. This code has the potential to identify fine-scale structure such as caustics in phase-space and the phase-space structure of tidal streams in the Milky-Way halo. Its ability to estimate the fine-grained $f(x;v)$ makes it useful for understanding non-equilibrium systems and for making accurate predictions for direct DM searches.

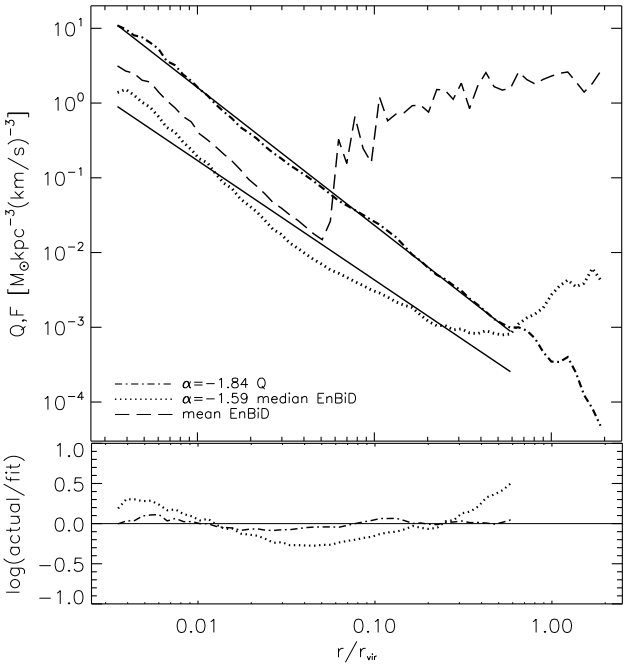

Figure 1. $Q(r)$ and $F(r)$ in 100 spherical radial bins about the most-bound-particle in halo G_1 from the $L25$ simulation at z=0. Top panel: Q (dot-dashed curve); power-law fit $Q / r^{1:84 \quad 0:012}$ is given by upper thin solid line. $F(r)$ from EnBiD (with $n = 10$ smoothing kernel (dotted curve)); power-law fit to $F(r) / r^{1:59 \quad 0:054}$ is given by lower thin solid line. Mean value of f (long-dashed curve) is noisier than $F(r)$ due to subhalos. Residuals to the two power-law fits are shown in the bottom panel.

For our halos at $z = 0$, the results we obtained with the different codes were completely consistent with those obtained by Sharma & Steinmetz (2006). The deviations between the estimates obtained with the different codes and various parameters were significantly higher at higher redshift - where comparisons with analytic estimates are not available. We refer the reader to the Appendix for a detailed comparison between estimated values of f using the two codes at various redshifts. In the rest of this paper we present results obtained with EnBiD ($n = 10$ kernel), the parameters preferred by Sharma & Steinmetz (2006).

Figure 1 *Top* shows the spherically averaged quantity $Q = \langle f \rangle = \int^3$ (dot-dashed curve); the mean of $f(x;v)$ in spherical bins (dashed curve) and the median DF in spherical bins (dotted curve). As we will show in Figure 4, the large fluctuations in the mean value of f (dashed curve) beyond $0{:}1 r_{vir}$ are due to the presence of substructure, which can have extremely high central values of f. The median value of f (hereafter represented by F) is much smoother, being less sensitive to the large range (nearly eight orders of magnitude) in f at each radius. In what follows, we will

use the median f, computed in concentric radial bins centered on the most bound particle in the main halo, since it is less sensitive to substructure. $Q(r)$ is well fitted by a power-law: $Q \propto r^{1.84\ 0.012}$ over the radial range $[0.004-0.6]\,r/r_{vir}$ (upper thin solid line). The power-law fit $F(r) \propto r^{1.59\ 0.054}$ over the same radial range is shown by the lower thin solid line. The bottom panel shows the residuals of the fits F ($\log(F/F_t)$) and Q ($\log(Q/Q_t)$). This plot shows that while $Q(r)$ is an extremely good power-law, the median $F(r)$ is only approximately power-law over the same radial range. Note that $Q(r)$ is numerically larger than $F(r)$ due to the fact that the former quantity does not properly account for the volume of the phase-space element. A similar result was obtained in a much higher resolution simulation by Stadel et al. (2008), a study which appeared as we were preparing this paper for publication.

3 EVOLUTION OF PHASE-SPACE DENSITY WITH REDSHIFT

Hoffman et al. (2007) studied the phase-space density profiles of a DM halo by tracking $Q(r)$ for material within the formal virial radius at each redshift. They found that the virialized material within this radius has an approximately power-law form with a constant power-law index of $1.9 \quad 0.05$ at all redshifts from $z = 5$ to the present.

We follow a slightly different approach in this paper, since our objective is to understand the evolution of the true coarse-grained phase-space density distribution. We track the evolution of phase-space density, by tracing backwards in time, all the material that lies inside the virial radius at $z = 0$. This will allow us to understand how the initially high phase-space density material that lies outside virialized systems at high redshift falls in and undergoes mixing and how the resultant mixing preserves the phase-space density profiles as a function of redshift.

We identified Milky-Way sized DM halos at $z = 0$ in our cosmological simulations and identify all the particles that lie inside twice the virial radius at $z = 0$. Our choice of halo outer radius ($2r_{vir}$) is motivated by the recent work of Cuesta et al. (2008) who showed that the virial radius is arbitrary and does not correspond to a physically meaningful outer boundary for a DM halo. A better *outer* radius is the so-called "static radius", defined as the radius at which the mean radial velocity of particles is zero. This radius is typically about $2r_{vir}$ for a galaxy-sized DM halo. After identifying all particles within $2r_{vir}$ at $z = 0$, we tracked them back to $z = 9$. Our simulations do proceed back in time to even higher redshifts, however we do not analyze them here because the mass resolution at higher redshifts does not allow us to resolve the evolution of most of the objects beyond this epoch. There were $1.6 \quad 10^6$ particles within 2 virial radii of the G_1 halo, which is the halo that is most isolated at $z = 0$. Two other halos (G_2 and G_3) from the $L25$ simulation are closer to each other at $z = 0$ (1.5 virial radii apart). Therefore, we only tracked those particles which lay within one virial radius of the centers of these two halos at $z = 0$ back in time to $z = 9$. The particles in the high resolution simulation $L20$ were selected and tracked in the same way as for the G_1 halo, and at $z = 0$ there were $3 \quad 10^6$ particles inside twice the virial radius. The position and velocity data for all the particles identified as belonging to a given halo at $z = 0$ were analysed.

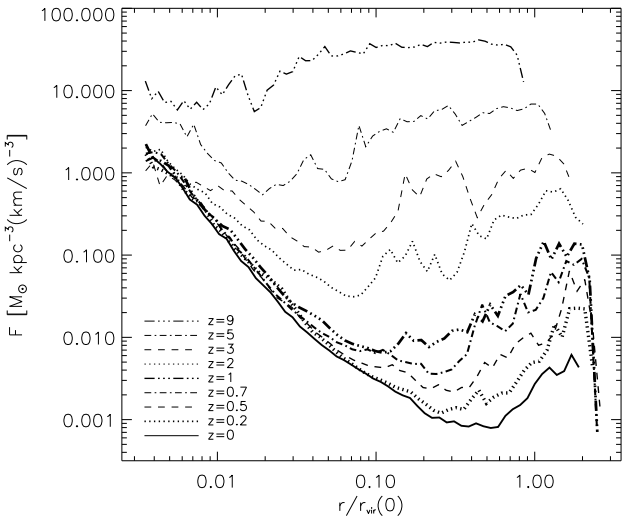

Figure 2. F as a function of comoving radius r for all material that lies within $2r_{vir}$ of the center of the G_1 halo at $z = 0$. Each curve corresponds to a different redshift as indicated in the legends.

At all redshifts we compute the phase-space densities of particles in *physical coordinates* rather than in co-moving coordinates. Distances are always in kpc and velocities are in km s^{-1}, and these quantities are measured relative to the center of the most massive progenitor. In many of the figures that follow, the physical distances at all redshifts other than $z = 0$ are scaled by the virial radius at $z = 0$; i.e. all distances are given in units of $r/r_{vir(z=0)}$.

In this section, we will present the results obtained for the G_1 halo in the $L25$ simulation. A comparison with results for the other three halos is made in §4.

Figure 2 plots the median value (F) of the phase space density f as a function of radius (as defined above) at several different redshifts. At the highest redshift plotted ($z = 9$), the overall value of F is higher at large radii than it is at the center of the halo, and it only varies by a factor of few over the entire range of radii ($F \quad 10 \quad 30 M_\odot\ \mathrm{kpc}^{-3}(\mathrm{km\ s}^{-1})^{-3}$). This is because within the inner, virialized regions the coarse-grained phase-space density is lowered due to mixing, while it is still high in the outer regions where the large fraction of matter is not yet mixed or is located in small subhalos, that have not mixed to the same degree as the main host. As the evolution progresses, there is a decrease in the central value of F till $z = 3$. The median value of F at the center of the

halo drops from $F \sim 10M_\odot\ \mathrm{kpc}^{-3}(\mathrm{km\ s}^{-1})^{-3}$ at $z = 9$ down to $F \sim 2M_\odot\ \mathrm{kpc}^{-3}(\mathrm{km\ s}^{-1})^{-3}$ at $z = 0$. The central value of F remains constant beyond $z = 3$, while there is a steady decrease in F at intermediate radii.

Although it is instructive to plot the mean and/or median values of F at each radius, much more information is contained in the full coarse-grained phase-space density f. The six-dimensional function $f(x;v)$ can be most easily visualized using the volume DF $V(f)$, which also obeys a Mixing Theorem (Mathur 1988). Arad et al. (2004) showed that at $z = 0$, $V(f)$ for cosmological DM halos follows a power-law profile $V(f) \propto f^{-\alpha}$ with power-law index $\alpha = 2.4$ over four orders of magnitude in f. They argued that since DM halos are almost spherical, if their phase-space DFs are approximately isotropic, their DFs could be written as functions of energy alone: $f = f(E)$. In this case they showed that if $Q \propto r^{\beta}$, then $V(f)$ would also be described by a power-law, and the index α was related to the index β through a simple equation.

In Figure 3 we plot the evolution of $V(f)$ with redshift for all the material that lies within twice the virial radius of halo G_1 at $z = 0$. In the bottom right-hand panel, the solid line is a fit to $V(f)$ for values of $10^{-4} < f < 10^{2.5}$. Over this range the best fit power-law profile is given by $V(f) \propto f^{-2.34\pm0.02}$ which is not very different from the power-law profile fit obtained by Arad et al. (2004). At all redshifts $V(f)$ deviates from the power-law profile at both low and high end. It is likely that at the high-f end the distribution deviates from the power-law due to the unresolved subhalos below the mass resolution limit of the simulation.

The *Mixing Theorem* requires that the coarse-grained volume distribution function $V(f)$ always *increases* (Mathur 1988). We see that $V(f)$ increases steadily from $z = 9$ onward for $f < 1M_\odot\ \mathrm{kpc}^{-3}(\mathrm{km\ s}^{-1})^{-3}$ in such a way that as the system evolves, there is more volume associated with material with low f. At higher values of f, $V(f)$ remains almost constant with decreasing redshift, probably owing to the fact that this material forms the cusps of DM halos. While the Mixing Theorems have previously been demonstrated for isolated systems, this is to our knowledge the first demonstration of their validity in a cosmological context.

It is particularly illuminating to plot the full coarse-grained phase space density of all particles as a function of radius from the center of mass of the main halo at each redshift (Figure 4). At any radius from the center there exist particles with phase-space densities spanning between 4-8 decades in f. The colored contours represent a constant particle number per unit area on the plane $(\log(f);\log(r))$. The yellow/orange contours represent the parameter range with the largest number of particles, while the blue/black contours represent regions with the smallest number of particles. The solid white curves on each plot show the median value (F) of $f(x;v)$ in 100 logarithmically spaced bins in r. These curves are identical to the various curves in Figure 2 and trace the regions with the largest particle number density at each radius. Numerous spikes in f are seen at $r > 0.1r_{vir}$ and correspond to DM sub-halos.

As the evolution proceeds, there is an overall lowering of the median phase-space density F (white curves). There is also a continuous decrease of the low-end envelope of f to lower values pointing to an increasingly large amount of matter with low phase-space density. However the upper envelope representing the highest phase space density regions at the centers of the subhalos remains relatively unchanged with redshift, indicating that primordial values of f are largely preserved at the centers of DM subhalos lying outside the center of the main halo.

It is illustrative to compare the evolution of $F(r)$ and $Q(r)$ with redshift. Figure 5 shows the two curves plotted as a function of radius (in comoving units) at each redshift for all the matter in halo G_1 that lies within two virial radii at $z = 0$, as a function of physical radius from the center of the most massive progenitor of the final halo (in units of the virial radius at $z = 0$). In each panel a thin vertical line is drawn at *the virial radius of the halo at that redshift*.

We find the best fit power-law $Q \propto r^{-1.84\pm0.012}$ at $z = 0$ to the profile within $0.6r_{vir}$. In agreement with Hoffman et al. (2007), we find that the same power-law provides a reasonably good fit to the profiles at redshifts from $z \sim 5$ to $z = 0$. While Q always decreases with radius since it is a spatial average over increasingly large volumes of configuration space, the median phase-space density F decreases monotonically with radius only within about $0.6r_{vir}$ of the main progenitor at that redshift. Outside the virial radius at each redshift (i.e. to the right of the vertical dashed line), $F(r)$ become significantly flatter, even increasing with increasing radius. At all $z \lesssim 6$ this represents the median phase-space density of matter that will lie within the outer radius of the halo at $z = 0$, but is either still unvirialized or lies within small halos. In general this material is not as mixed as the more massive main progenitor. The nearly constant value of F beyond the virial radius at high z may be interpreted as the median phase-space density of DM in the Universe at that redshift. At lower redshifts, a non-negligible fraction of this matter lies within inner regions of small halos, which have undergone relatively small amount of mixing. As more and more material undergoes substantial mixing as the halos evolve, the high phase-space density unmixed material in the subhalo centers, as well as in the relatively unmixed streams formed from disrupted subhalos, prevents the median at large radii from decreasing rapidly, despite the large increase in low material with low f-values within the virialized regions of the main halo.

To better understand the evolution of f with redshift we plot histograms of $\log(f)$ at each redshift in Figure 6 (thick solid histograms). The thin red curves at each redshift represent the best-fit Gaussians to the distribution of $\log(f)$ at that redshift. A Gaussian provides a good fit to the majority of the mass. (Since $\log(f)$ is close to Gaussian, f itself has a log-normal distribution.) By approximately $z = 1$, the skewness of the distribution is significant, and the skewness increases steadily until $z = 0$. To better understand the origin of the matter in the high-f tail at z=0, we plot the distribution of DM particles that have the values of $f > 1M_\odot\ \mathrm{kpc}^{-3}(\mathrm{km\ s}^{-1})^{-3}$ at $z = 0$. The ordinate values of

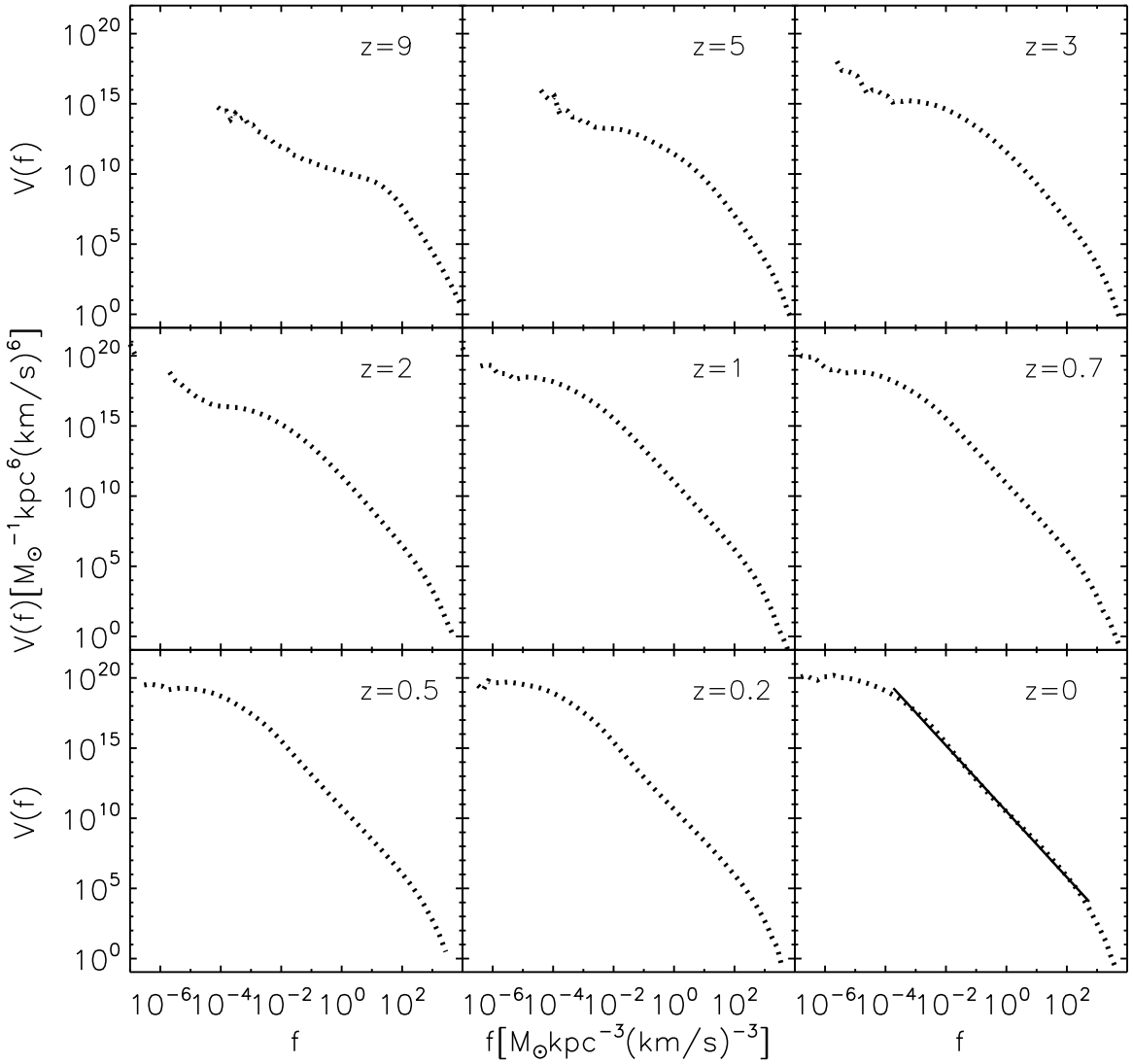

Figure 3. The volume DF V (f) for G 1 halo in the L 25 simulation at different redshifts. A power-law fit to V (f) / f 2:34 0:017, is shown at z = 0 (solid line).

this distribution (multiplied by a factor of 10 to enhance visibility), are shown in the dashed histograms. The thin blue curves show that the high-f tail is also well fitted by a Gaussian (except at z = 0). As we saw in Figure 4, most of these high-f tail particles are in subhalos at z = 0, while some are also in the highest phase-space density particles in the central cusp of the halo at z = 0. This high-f sub-population has a Gaussian distribution at z = 9 with a mean f = 1:73 0:6M kpc 3 (km s 1) 3 compared with the mean f = 1:57 0:54M kpc 3 (km s 1) 3 for all the particles (in the solid curve) at z = 9. A Students' T-test indicated with 99% confidence that both distributions are drawn from the same population at z = 9. This implies that the material that lies in the centers of DM subhalos at z = 0 will have phase-space densities that are representative of the mean phase-space density of matter at z = 9.

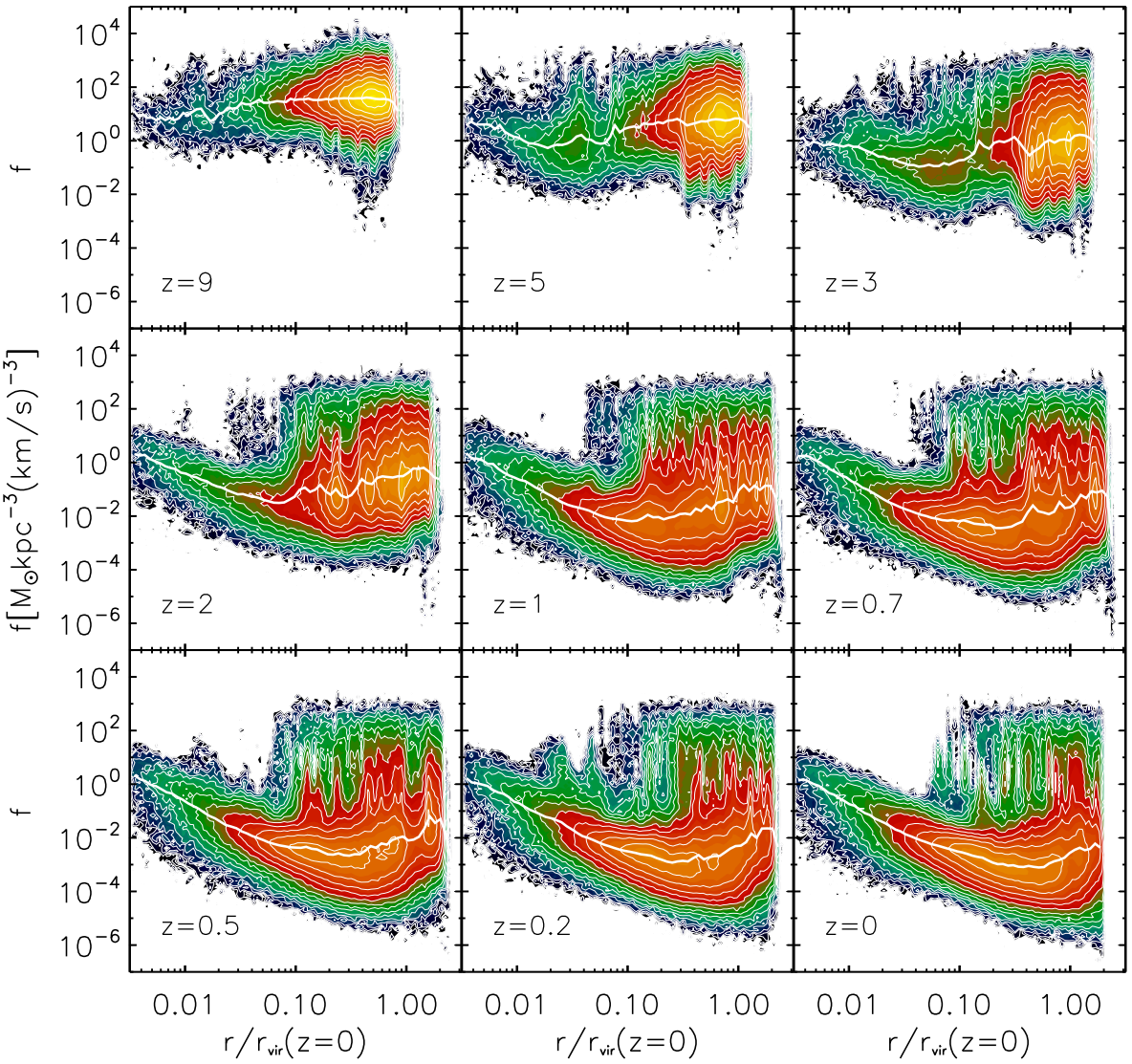

Figure 4. Contours of constant particle number density in the plane (log(f); log(r)) for the G 1 halo, plotted at different redshifts. At each redshift the radial distribution of particles is given relative to the most bound halo particle in units of the virial radius of the halo at z = 0. The yellow and black contours correspond to the regions with the highest and lowest particle number densities respectively. Contours are spaced at logarithmic intervals in particle number density relative to the maximum density contour. F , the median value of f at each radius is represented by the solid white line.

4 COMPARISON OF FOUR MILKY-WAY SIZED HALOS

In this section we present results for the phase-space DFs for all four of the DM halos described in x2. Although we present results mainly at z = 0, evolution with redshift for each of the halos were similar to the evolution of halo G 1 presented earlier.

Figure 7 compares the volume distribution of phase space density V (f) for the four different halos at z = 0. All three halos from the L25 simulation (G 1, G 2, G 3) show almost identical profiles in V (f) confirming the universality of the process that produced the phase-space DF. For halo L20, V (f) lies systematically above the other curves especially at higher values of f, where it also extends to large values of f. It was first shown by Sharma & Steinmetz (2006) that this is a numerical consequence of the increased mass resolution of the simulation. This indicates that the absolute value

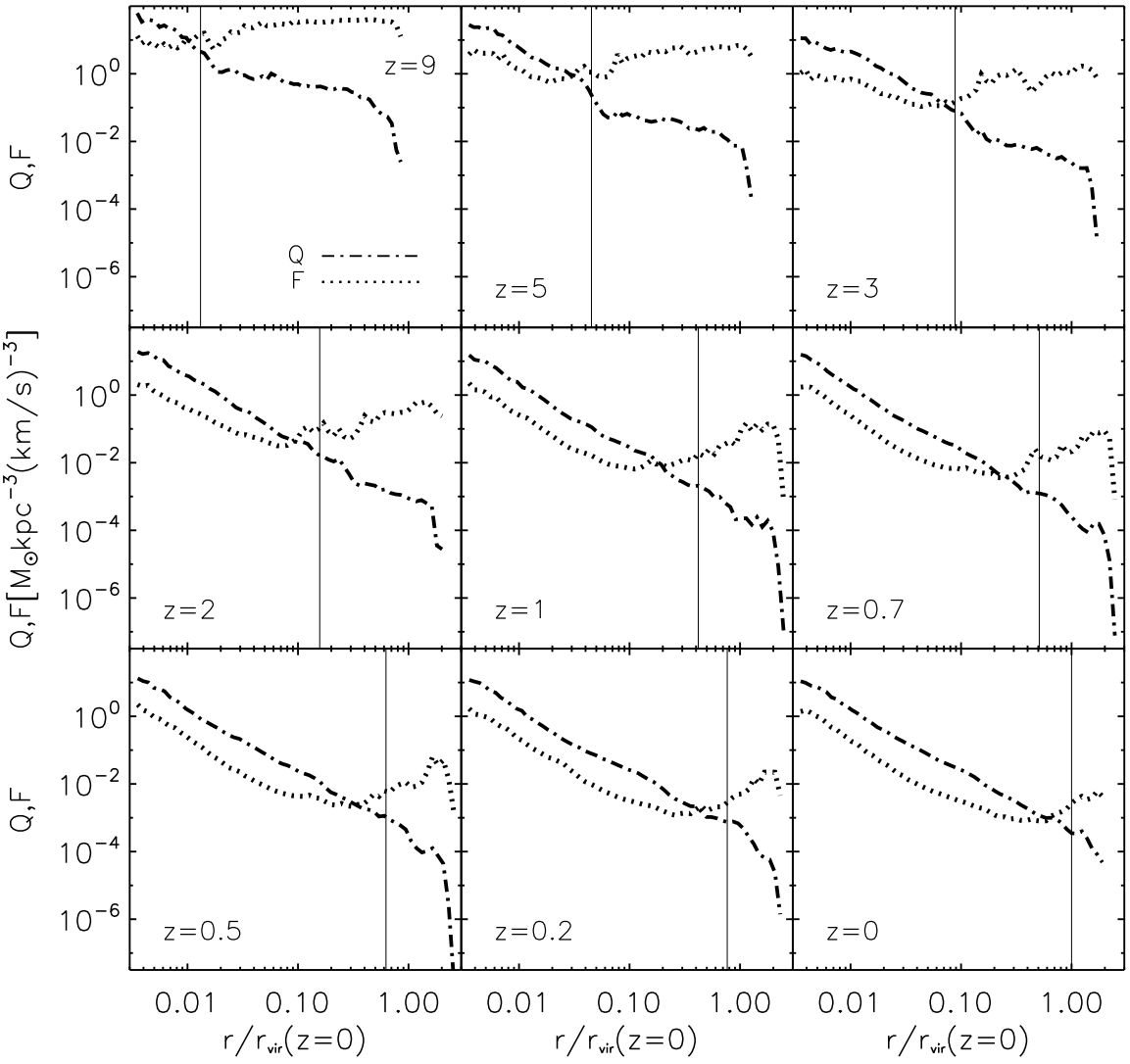

Figure 5. $Q = \ = {}^{3}$ (dot-dashed line) and median F (dotted line) as a function of $r{=}r_{vir}(z = 0)$ for different redshifts for the G_1 halo. The dashed vertical line is situated at the virial radius of the main halo at each redshift.

of f derived in the previous section is somewhat dependent on the mass resolution of the simulation and increases slightly with increasing mass resolution. In all four halos $V(f)$ is well approximated by a power-law over nearly six orders of magnitude in f. The first column of Table 1 gives details of the power-law fits to $V(f)$ (i.e. the power-law slopes and their errors over the range $10^{-4} < f < 10^{2:5}$.) The power-law slopes we obtained are similar to those obtained by previous authors (Arad et al. 2004).

In Figure 8 we plot $F(r)$ and $Q(r)$ for the four different halos at $z = 0$. The top set of four curves show $Q(r)$ while the lower set of curves show $F(r)$. In all four halos, $Q(r)$ is well fitted by a power-law of slope $= 1{:}8 \quad 1{:}9$ (see Table 1). $F(r)$ shows significant deviations from a simple power-law profile, with a systematic upturn beyond $r{=}r_{vir} > 0{:}1$. The higher resolution simulation (L20) appears to have systematically higher F and Q values than the halos from the low resolution simulation (again, a numerical consequence of the higher mass resolution Sharma & Steinmetz 2006). Table 1 gives the values for the slopes and the error-bars on the power-law fits to $Q(r)$ and $F(r)$ for $r < 0{:}6r_{vir}$ as well as the inner power-law slope of $F(r)$.

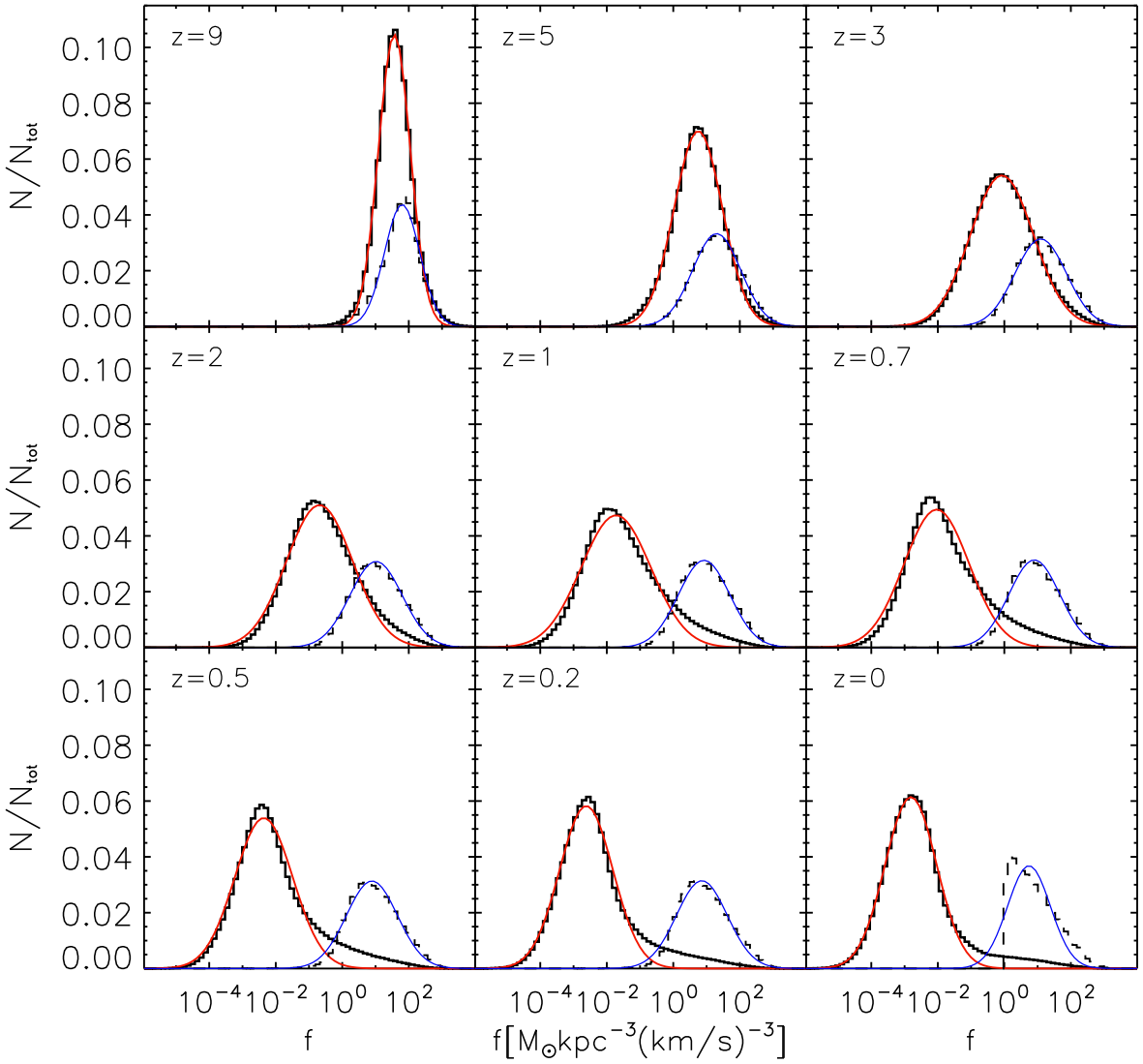

Figure 6. Histograms of the phase-space density f of all halo particles as a function of redshift (thick solid histograms). The dashed histograms follow those particles which have the highest phase-space densities f > 1 at z = 0, with ordinate values multiplied by 10 to enhance visibility. The thin red curves are the best-fit Gaussians to all the particles in the thick solid histograms, while the thin blue curves are best-fit Gaussians to dashed histograms.

Table 1. Power-law indices for fits to V , Q , and F for four halos at z = 0 for r < 0:6r_{vir}

Halo	V		Q		F	
G_1	2:34	0:02	1:84	0:01	1:59	0:05
G_2	2:37	0:02	1:82	0:01	1:46	0:06
G_3	2:35	0:02	1:75	0:01	1:42	0:03
L20	2:27	0:01	1:87	0:01	1:64	0:07

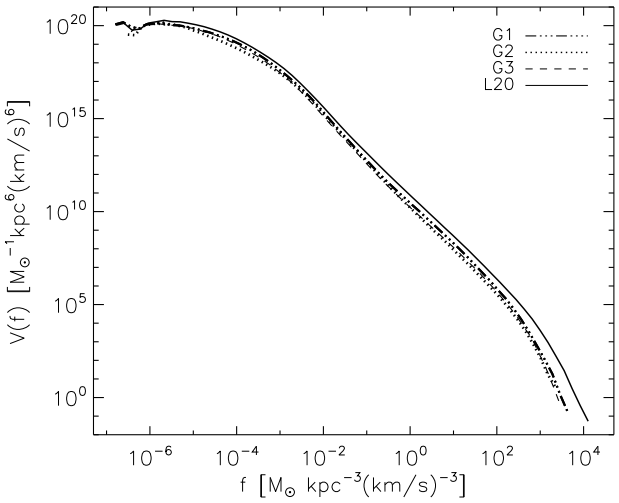

Figure 7. $V(f)$ for four halos, at $z = 0$. The triple-dot-dashed line is for $G1$, the dotted line for $G2$, the dashed line for $G3$, and the solid line is for higher mass resolution simulation $L20$.

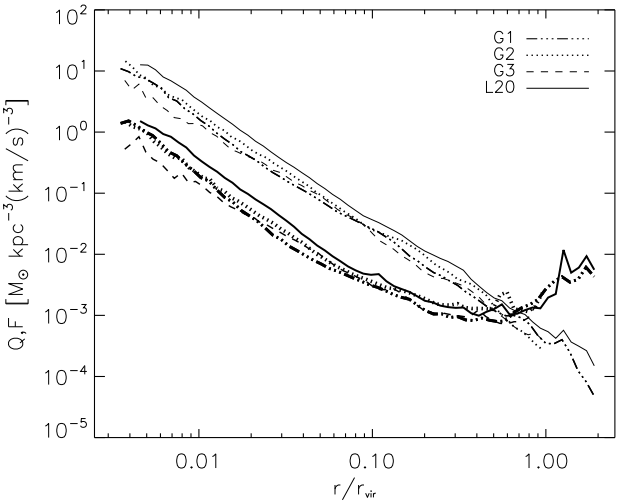

Figure 8. Q (thin lines) and F (thick lines) for all the halos studied, at $z = 0$. Triple-dot-dashed lines are for $G1$, dotted lines for $G2$, dashed lines for $G3$, and the solid lines are for $L20$.

5 DISCUSSION

Several previous studies have attempted to account for the origin of the power-law $Q(r)$ profiles of DM halos. Notably, it has been argued that power-law profiles result from virialization and not from the hierarchical sequence of mergers, since they are also produced in simple spherical gravitational collapse simulations (Taylor & Navarro 2001; Barnes et al. 2006, 2007). Our results presented in the previous section (Figure 5) show that while $Q(r)$ and $F(r)$ have approximately power-law form within $0.6r_{vir}$ at a given redshift, $F(r)$ flattens out and remains quite flat beyond this radius. Furthermore, as the hierarchical growth of the halo progresses these approximately power-law profiles extend to larger radii until they encompass all the mass within the virial radius at $z = 0$.

It has been shown from both theoretical arguments and numerical simulations (Dehnen 2005; Vass et al. 2009) that power-law profiles of phase-space density for central cusps are well preserved during major mergers. At intermediate times during a major merger, deviations from the power-law profile are seen but these largely disappear at the end of the merger. In major mergers there are two main reasons for the preservation of the power-law profiles. First, the most tightly bound material - that forming a steep central cusp or shallow core preserves its phase-space density in the final remnant. This is a consequence of the additivity of the excess mass function - a result of the fact that steeper cusps are less mixed than shallower cusps (Dehnen 2005). Over 60% of the material in the central cusp (within one scale radius) of a progenitor NFW halo remains within the cusp of the merger remnant (Valluri et al. 2007). The second reason for preservation of power-law profiles at large radii is that material outside three scale radii of the progenitor halos is redistributed to other radial bins almost uniformly from each radial interval. In addition, nearly 40% of the material within the virial radius of the progenitor halos is ejected to beyond the virial radius of the final remnant (Kazantzidis et al. 2006; Valluri et al. 2007). This material can be shown to have originated in roughly equal fractions from each radial interval beyond three scale radii and has higher phase-space density than expected from the simple power-law extrapolation of the inner power-law. This self-similar redistribution of material contributes to the preservation of power-law profiles in $Q(r)$ and $F(r)$ in equal mass binary mergers. Thus, once a power-law phase-space DF has been established in a DM halo, major mergers will not destroy this profile. This has been confirmed by our recent work on mergers of equal mass halos (Vass et al. 2009).

As discussed in the previous section (Figure 6), the coarse-grained phase-space density f in CDM halos has a nearly log-normal distribution with the median of $\log(f)$ (the peak of the histogram f_{peak}) evolving steadily toward lower values of f as the halo grows. We now quantify the evolution of f_{peak} with redshift.

Figure 9 shows the evolution of median phase-space density f_{peak} derived from the histograms of $\log(f)$ in Figure 6 for each of the 4 Milky-Way sized cosmological halos in this study. The solid dots represent the values of f_{peak} as a function a, while the dotted curves are meant to guide the eye by connecting points for each of the 4 individual halos. For $a < 0.5$ the decline in f_{peak} is approximately power-law: $f_{peak}(a) \propto a^{-4.5}$. This implies that the matter inside the halos has undergone significant mixing due to virialization during the hierarchical formation process, the leveling off of the curve at $a \gtrsim 0.5$ indicates a decrease in mixing after

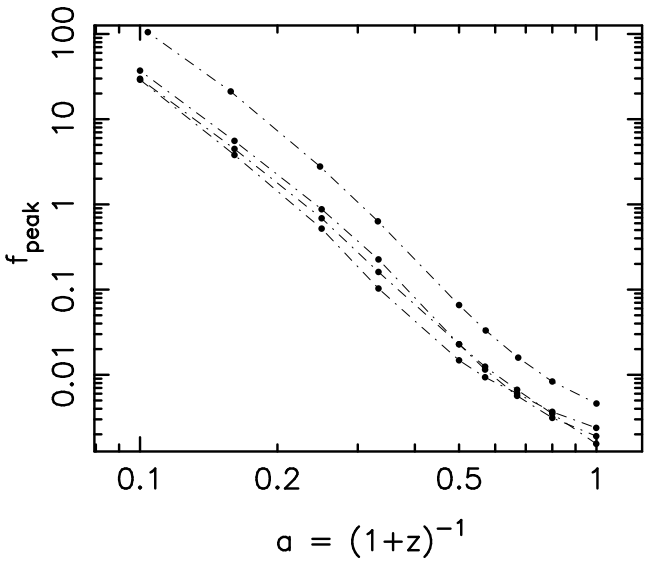

Figure 9. The median phase-space density (peak of histograms f_{peak} in Fig. 6) at each redshift as a function of the cosmic scale factor $a = (1 + z)^{-1}$, plotted for four Milky-way sized halos (points). The thin dotted lines connect points for the four individual halos.

$z = 1$, possibly resulting from a decrease in mass accreted in major mergers.

On average, as a halo grows via accretion its median density decreases as a power-law with time, despite the fact that the most centrally concentrated material retains its original high phase-space density. This nearly power-law profile in f_{peak} leads to some insights into the development of phase-space density profiles. We can break down the formation of halos into two phases (Li et al. 2007): the fast accretion regime during which halo mass grows very rapidly and the slow accretion regime. In the fast accretion regime, the mixing processes are very efficient as the potential well is established and potential fluctuates rapidly and constantly. This results in a rapid decrease in the overall central phase-space density of the halo (as seen from the rapid drop in the central most regions of the profiles in Fig. 2.) The inner profile of phase-space distribution should be largely set during this stage. As halos grow subsequently, either by major mergers or quiescent accretion of smaller halos, the average phase-space density decreases, but the pre-existing high central phase-space density cusps are preserved.

At these later times the evolution of the true phase-space density is complex and occurs due to the accretion of high phase-space density material in subhalos, as well as loosely bound material at the edges of the halo. The steady decrease in the amplitude and increase in the slope of the $F(r)$ profiles in Fig. 2 with redshift show that the true phase-space density does not obey the power-law profiles seen in $Q(r)$ at all redshifts. Variations in the individual power-law profiles of halos both at $z = 0$ (Fig. 8) and with redshift reflect the large variation in the cosmic accretion histories of individual halos. Additional deviations from the power-law arise due to the matter bound to subhalos that survives with high phase-space density and leads to the variation of the coarse-grained f of some six orders of magnitude in the outer regions of halos.

All this indicates that the actual phase-space distribution is not as universal and simple as the $Q(r)$ profiles lead one to believe. The mechanism behind the universal power-law form of the $Q(r)$ profiles is therefore likely to be different (e.g., it is not affected by the presence of subhalos) and simpler than the processes that shape the distribution of the coarse-grained phase-space density. The Q profile is a ratio of the density and velocity dispersion (which can be interpreted as a measure of temperature) and is therefore related to the entropy. For an ideal monatomic gas the entropy can be defined as $K_{gas} = T/^{2/3}$, while for DM, by analogy, the entropy can be defined as $K_{dm} = \sigma^2/\rho_{dm}^{2/3}$ (Faltenbacher et al. 2007). This, as noted by Hoffman et al. (2007), gives $K_{dm} / Q^{2/3}$ or $K_{dm} / r^{1.2}$ for $Q / r^{1.8}$. This power-law form and slope of the entropy profile is very similar[2] to the one found for the gas in the outer regions of clusters in cosmological simulations (e.g., Borgani et al. 2004; Voit et al. 2005). This power-law is also predicted by the models of spherical accretion (Tozzi & Norman 2001) and reflects the increasing entropy to which the accreting material is heated as the halo grows its mass. Although the processes governing the virialization of gas and DM are different (the short-range local interactions for the former, and long-scale interactions for the latter), the fact that the resulting entropy profiles are quite similar indicate that they lead to the same distribution of entropy. The $Q(r)$ profile therefore may reflect the overall entropy profile of DM, not the coarse-grained local phase-space density, which exhibits a more complicated behavior.

6 SUMMARY AND CONCLUSIONS

We have investigated the evolution of the phase-space density of the DM in cosmological simulations of the formation of Milky-Way-sized DM halos. The analysis was carried out using two different codes for estimating the phase-space density. Both codes give qualitatively similar results, but the estimated values of phase- space density f are quite sensitive to the type of code and, for a given code, also depend quite sensitively on the choice of smoothing kernel used. Based on comparisons of the two codes (FiEstAS and EnBiD) and various smoothing parameters (Appendix), we select the EnBiD code with $n = 10$ kernel smoothing and present results for the analysis with this set of parameters.

[2] The slope is even more similar if one takes into account the random bulk motions of the gas in estimating K_{gas} (Faltenbacher et al. 2007).

The simulations presented in this paper complement our analysis of the evolution of phase-space density in binary major mergers (Vass et al. 2009). We confirm that the profiles of $Q(r) = {}_{dm} = {}^{3}_{dm}$ computed by previous authors can be described by a power-law $Q(r) / r^{1:8\ 0:1}$ over more than two orders of magnitude in radius in all halos. The median of the phase-space density ($F(r)$) at given radius r, however, exhibits a more complicated behavior. Although $F(r)$ is approximately a power-law for $r < 0{:}6r_{vir}$, the profiles generally flatten in the outer regions. Subhalos contribute somewhat to this behavior, although their effect is limited by the relatively small fraction of mass ($< 0{:}1$) bound to them. However, in addition to subhalos, a significant fraction of high phase-space density matter is in the relatively unmixed material (possibly in streams) arising from tidally disrupted subhalos (e.g., Arad et al. 2004; Diemand et al. 2008). The rise in $F(r)$ at large radii suggests that the fraction of mass in such streams can be substantial.

This behavior holds at earlier epochs. From $z = 5$ to $z = 0$, material within $r_{vir}(z)$ at each redshift follows a power-law in Q with an approximate power-law slope of $1{:}8$ to $1{:}9$. In contrast, $F(r)$ can only be well described by a power-law in the inner regions, and its slope changes continuously with redshift. Beyond the virial radius, Q (a quantity that is obtained by averaging over increasingly large volumes) decreases rapidly with radius, but the median value of F flattens significantly. We argue that F is a more physically meaningful quantity, especially for understanding the evolution of phase-space density in collisionless DM halos, as it measures the median of the true coarse-grained phase-space density.

At all redshifts, the highest values of phase-space density f are found at the centers of DM subhalos. In the center of the main halo, the median phase-space density (F) drops by about an order of magnitude from $z = 9$ to $z = 0$. In contrast, the centers of DM subhalos maintain their high values of $f \quad 10^{3}M \quad kpc^{\ 3}(km\ s^{\ 1})^{\ 3}$ at all redshifts. The highest values of f at the center of the main halo are, therefore, lower and less representative of the primordial phase-space density of DM particles than the central value of f in the high phase-space density subhalos. At r_{vir}, the decrease in median phase-space density is much more significant, with $F \quad 30M \quad kpc^{\ 3}(km\ s^{\ 1})^{\ 3}$ at $z = 9$ decreasing to $F \quad 10^{\ 3}M \quad kpc^{\ 3}(km\ s^{\ 1})^{\ 3}$ at $z = 0$, a decrease of over four orders of magnitude (Figure 4).

The evolution of $F(r)$ and $V(f)$ with redshift are consistent with expectations from the Mixing Theorems, which require that mixing reduces the overall phase-space density of matter in collisionless systems and that the volume of phase-space associated with any value of f increases due to mixing and relaxation.

The distribution of f is approximately log-normal until $z \quad 3$. As time progresses, the mean and median of $\log(f)$ shift to progressively lower values as a larger and larger fraction of matter undergoes mixing and moves to lower values of f. Some fraction of high phase-space density material does survive in the centers of subhalos and in the relatively unmixed streams leftover after subhalo disruptions, which skews the distribution. Remarkably, the highest phase-space density particles at $z = 0$ have retained their phase-space density since $z \quad 9$, the earliest epoch we analyzed. The phase-space density in the centers of DM subhalos is therefore representative of the mean phase-space density of DM at the highest redshifts. This can potentially allow for stronger constraints to be placed on the nature of DM particles from the Tremaine-Gunn bound (Tremaine & Gunn 1979; Hogan & Dalcanton 2000).

The median value of phase-space density decreases with decreasing redshift approximately as a power-law described by $f_{peak} \ ' \ a^{\ 4:5}$. This majority of the decrease in f_{peak}, is the result of mixing within virialized halos which reduces the coarse-grained phase-space density of matter that has turned around from the Hubble flow, much of this mixing occurs prior to $z \quad 1$, after which the rate of mixing in galactic sized halos slows down.

ACKNOWLEDGMENTS

We thank Y. Ascasibar and S. Sharma for the use of the FiEstAS code and EnBiD code, respectively. We especially thank S. Sharma for detailed discussions on his EnBiD code. We thank the referee Stephane Colombi for his helpful comments. IMV would like to thank Stephen T. Gottesman for valuable input during the early stages of this work, and acknowledges the support of National Science Foundation (NSF) grant AST-0307351 to the University of Florida. IMV, MV, AVK, and SK were supported in part by Kavli Institute for Cosmological Physics at the University of Chicago (where most of this work was carried out) through grants NSF PHY-0114422 and NSF PHY-0551142 and an endowment from the Kavli Foundation and its founder Fred Kavli. MV is also supported by the the University of Michigan. AVK is also supported by the NSF under grants AST-0239759 and AST-0507666 and by NASA through grant NAG5-13274. AVK would like to thank the Kavli Institute for Theoretical Physics, supported in part by the NSF under grant PHY05-51164, for hospitality during the final editing of the paper and participants of the workshop "Back to the Galaxy" for useful discussions and feedback on the results of this paper. SK is supported by the Center for Cosmology and Astro-Particle Physics (CCAPP) at The Ohio State University.

APPENDIX A: COMPARISON OF "FiEstAS" AND "EnBiD" ANALYSIS OF HALO G_1

The numerical estimation of coarse-grained phase-space densities during the evolution of the four N-body halos presented in this paper was carried out using two publicly available codes "FiEstAS" (Ascasibar & Binney 2005) and "EnBiD" (Sharma & Steinmetz

2006). A comparison of these two codes has previously been presented by Sharma & Steinmetz (2006), who showed for an analytic DF (for the spherical Hernquist potential), that "EnBiD with n = 10 kernel smoothing" gave the highest fidelity to the analytical DF. In a related work Vass et al. (2009) confirmed the findings of Sharma & Steinmetz (2006) for a spherical isotropic NFW halo. This latter study is the main basis for our choice of EnBiD with n = 10 kernel smoothing. After this paper was submitted to the Journal we became aware of the work of Maciejewski et al. (2008). These authors carried out a similar, and somewhat more detailed comparison, of coarse-grained phase-space density estimators for N-body simulations on cosmological halos at z = 0. Our results are in agreement with theirs.

However, it is unclear whether the comparisons with analytic profiles of isolated halos at z = 0 are valid for matter distributions arising from cosmological N-body distributions, at high redshifts, where the majority of the particles actually lie outside virialized halos. Our purpose in this Appendix is to present a comparison of results obtained with the different codes at a range of redshifts to allow readers to appreciate how sensitive some of the results presented in this paper are to the choice of code and smoothing parameters used in density estimation. Since the coarse-grained DF f(x;v) is a 6-dimensional function, it is difficult to compare estimates for this function obtained using different codes. Traditionally the best single variable function to compare is the volume DF V(f). Variations in the estimation of f translate to variations in estimation of V(f). In Figure A1 we compare the volume density of phase-space V(f) obtained for the G_1 halo at four different redshifts using the FiEstAS code (triple-dot-dashed curves), EnBiD code with no smoothing (dot-dashed curves), EnBiD with FiEstAS smoothing (long-dashed curves), and EnBiD with a n = 10 kernel (dotted curves). In each case we see that V(f) has a nearly power-law distribution over more than six orders of magnitude in f at z = 0 (from 10^{4}–10^{3} M kpc^{3} (km s^{1})^{3}). Table A1 gives the slopes of power-law fits for the four different estimates of V(f) over the range $10^{4} < f < 10^{3}$ at z = 0. The FiEstAS estimate of V(f) is systematically lower than all EnBiD estimates at high values of f (at all redshifts). In addition all EnBiD curves extend to much higher values of f than the FiEstAS estimate (this is particularly true at z = 9 where the FiEstAS estimate differs from the other estimates both quantitatively and qualitatively). The results from the various EnBiD estimates differ very little at intermediate values of f (10^{4}–10^{3}) and consequently we are confident that conclusions drawn from the median f is quite insensitive to the details of the EnBiD parameters used to obtain f.

The differences between the various estimates of F at large radii become significantly larger at higher redshift. In Figure A2 we plot the four different estimates of F(r) at four different redshifts in the evolution. The vertical dashed line in each panel represents the virial radius of the main halo at that redshift. We see that F from any of the codes is quite flat beyond the virial radius in all cases,

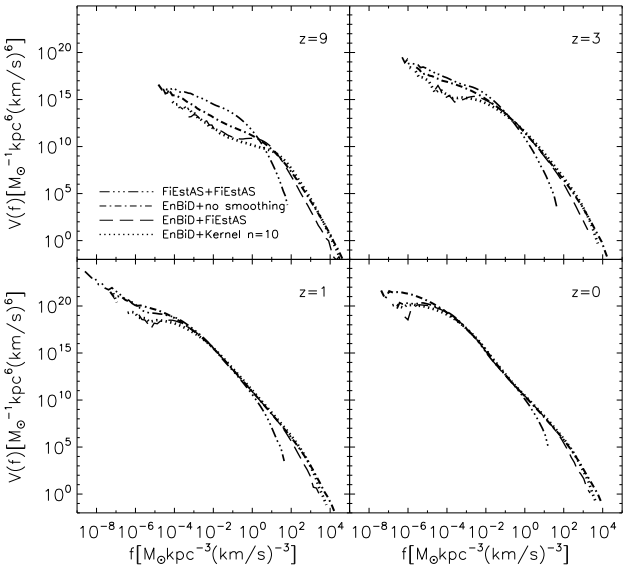

Figure A1. The volume DF V(f), at different redshifts during the evolution of the G_1 halo in the L25 simulation. Plots compare results obtained with the FiEstAS code and EnBiD code (using three different parameters) as indicated in the line legends.

Table A1. Power-law indices V(f) / f and F(r) / r at z = 0 from different codes

Code				
FiEstAS	2:62	0:06	1:43	0:02
EnBiD (no smoothing)	2:35	0:02	1:65	0:02
EnBiD (FiEstAS smoothing)	2:46	0:03	1:69	0:07
EnBiD (kernel n = 10)	2:34	0:02	1:59	0:05

but the absolute values of the curves differ significantly. Note that at z = 9, the different estimates can differ by as much as two orders of magnitude.

In this paper we choose to present results from EnBiD with n = 10 kernel smoothing over the other estimates largely because it does the best job of reproducing analytic DFs (Sharma & Steinmetz 2006) and because it appears to provide a good upper limit to the phase-space density both at high and low values of f. In the absence of an analytic comparison of the estimates at high redshift, we caution the reader to refrain from drawing very strong conclusions regarding absolute values of f or F from the results presented here.

REFERENCES

Arad I., Dekel A., Klypin A., 2004, MNRAS, 353, 15

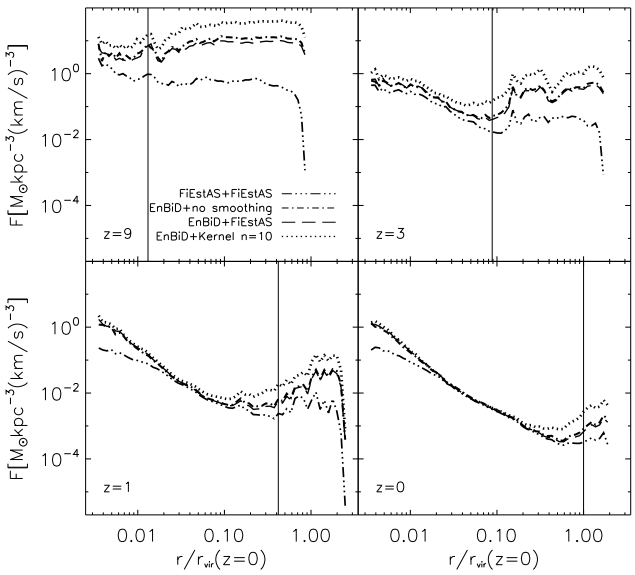

Figure A2. F for the G 1 halo in the L25 simulation at different redshifts obtained using FiEstAS and EnBiD as indicated by line-legends. The dashed vertical line is situated at the virial radius of the main halo at each redshift.

Ascasibar Y., Binney J., 2005, MNRAS, 356, 872

Ascasibar Y., Yepes G., Gottlöber S., Müller V., 2004, MNRAS, 352, 1109

Austin C. G., Williams L. L. R., Barnes E. I., Babul A., Dalcanton J. J., 2005, ApJ, 634, 756

Barnes E. I., Williams L. L. R., Babul A., Dalcanton J. J., 2006, ApJ, 643, 797

Barnes E. I., Williams L. L. R., Babul A., Dalcanton J. J., 2007, ApJ, 654, 814

Bertschinger E., 1985, ApJS, 58, 39

Binney J., Tremaine S., 1987, Galactic dynamics. Princeton, NJ, Princeton University Press, 1987, 747 p.

Borgani S., Murante G., Springel V., Diaferio A., Dolag K., Moscardini L., Tormen G., Tornatore L., Tozzi P., 2004, MNRAS, 348, 1078

Cuesta A. J., Prada F., Klypin A., Moles M., 2008, MNRAS, 389, 385

Dehnen W., 2005, MNRAS, 360, 892

Dehnen W., McLaughlin D. E., 2005, MNRAS, 363, 1057

Diemand J., Kuhlen M., Madau P., Zemp M., Moore B., Potter D., Stadel J., 2008, Nature, 454, 735

Faltenbacher A., Hoffman Y., Gottlöber S., Yepes G., 2007, MNRAS, 376, 1327

Gnedin N. Y., Kravtsov A. V., 2006, ApJ, 645, 1054

Hoffman Y., Romano-Díaz E., Shlosman I., Heller C., 2007, ApJ, 671, 1108

Hogan C. J., Dalcanton J. J., 2000, Phys. Rev. D, 62, 063511

Kazantzidis S., Zentner A. R., Kravtsov A. V., 2006, ApJ, 641, 647

Klypin A., Zhao H., Somerville R. S., 2002, ApJ, 573, 597

Knollmann S. R., Knebe A., Hoffman Y., 2008, MNRAS submitted (astro-ph/0809.1439), 809

Kravtsov A. V., Gnedin O. Y., Klypin A. A., 2004, ApJ, 609, 482

Kravtsov A. V., Klypin A. A., Khokhlov A. M., 1997, ApJS, 111, 73

Li Y., Mo H. J., van den Bosch F. C., Lin W. P., 2007, MNRAS, 379, 689

Maciejewski M., Colombi S., Alard C., Bouchet F., Pichon C., 2008, ArXiv e-prints

Mathur S. D., 1988, MNRAS, 231, 367

Merritt D., Graham A., Moore B., Diemand J., Terzić B., 2006, AJ, 132, 2685

Navarro J. F., Frenk C. S., White S. D. M., 1996, ApJ, 462, 563

Peirani S., de Freitas Pacheco J. A., 2007, ApJ submitted (astro-ph/0701292)

Rasia E., Tormen G., Moscardini L., 2004, MNRAS, 351, 237

Sharma S., Steinmetz M., 2006, MNRAS, 373, 1293

Stadel J., Potter D., Moore B., Diemand J., Madau P., Zemp M., Kuhlen M., Quilis V., 2008, ArXiv e-prints, 808

Taylor J. E., Navarro J. F., 2001, ApJ, 563, 483

Tozzi P., Norman C., 2001, ApJ, 546, 63

Tremaine S., Gunn J. E., 1979, Physical Review Letters, 42, 407

Tremaine S., Henon M., Lynden-Bell D., 1986, MNRAS, 219, 285

Valluri M., Vass I. M., Kazantzidis S., Kravtsov A. V., Bohn C. L., 2007, ApJ, 658, 731

Vass I. M., Kazantzidis S., Valluri M., Kravtsov A. V., 2009, ApJ

Vogelsberger M., White S. D. M., Helmi A., Springel V., 2008, MNRAS, 385, 236

Voit G. M., Kay S. T., Bryan G. L., 2005, MNRAS, 364, 909

Wang J., White S. D. M., 2008, MNRAS submitted (astro-ph/0809.1322), 809

Wojtak R., Łokas E. L., Mamon G. A., Gottlöber S., Klypin A., Hoffman Y., 2008, MNRAS, 388, 815

This paper has been typeset from a TEX/ LATEX file prepared by the author.